Geothermics xxx (2015) xxx–xxx

Contents lists available at ScienceDirect

Geothermics

journal homepage: www.elsevier.com/locate/geothermics

Mathematical modelling of fines migration in geothermal reservoirs

Zhenjiang You[a,*], Yulong Yang[a], Alexander Badalyan[a], Pavel Bedrikovetsky[a], Martin Hand[b]

[a] Australian School of Petroleum, The University of Adelaide, Adelaide, SA 5005, Australia
[b] South Australian Centre for Geothermal Energy Research, Institute of Mineral and Energy Resources, The University of Adelaide, Adelaide, SA 5005, Australia

ARTICLE INFO

Article history:
Received 4 September 2014
Accepted 25 May 2015
Available online xxx

Keywords:
Permeability reduction
Formation damage
Fines migration
Mathematical model
Slow particle motion

ABSTRACT

Laboratory-based mathematical modelling of fines migration allows predicting well productivity reduction during the geothermal reservoir exploitation. The analytical model for one-dimensional flow with ionic strength alteration has been derived. Good adjustment of the permeability and breakthrough concentration data from coreflood test by the analytical model has been achieved, and the tuned model coefficients fall in the common ranges. The obtained maximum retention function of multi-sized fines allows calculating their size distribution. During the temperature rise, weakening of electrostatic attraction on fines attached to rock surface overwhelms the reduction of detaching drag force due to water viscosity decrease. It leads to increased fines detachment and more severe permeability decline at elevated temperatures, typical for geothermal fields.

1. Introduction

Transport of suspensions and colloids in porous media with particle capture and permeability decline occurs in several processes of geothermal reservoir and production engineering, such as production of hot water from geothermal wells, enhanced geothermal systems with cold water injection and hot water/steam production, seasonal hot water storage in aquifers, etc. (Priisholm et al., 1987; Baudracco, 1990; Baudracco and Aoubouazza, 1995; Ghassemi and Zhou, 2011; Aragón-Aguilar et al., 2013; Rosenbrand et al., 2012, 2013, 2014, , 2015). The mathematical modelling of deep bed filtration accounting for particle capture, detachment and rock clogging is an essential part of the planning and design of the above-mentioned processes.

Since the particle capture by straining is the main physical mechanism of permeability damage during fines migration, and size exclusion is defined by pore and particle sizes, the micro scale models accounting for pore and particle size distributions are adequate for fines migration prediction (see micro scale schematic of fines mobilisation, migration and straining in Fig. 1). The detailed description of fines migration accounting for pore and particle size distributions can be performed by using the micro scale models of random walks (Cortis et al., 2006; Shapiro, 2007; Yuan and Shapiro, 2011), population balance models (Sharma and Yortsos, 1987a,b; You et al., 2013) and Boltzmann's physical kinetics equation (Shapiro and Wesselingh, 2008). However, to the best of our knowledge, the data on particle and pore size distributions during fines migration are not available in the literature. Therefore, the averaged equations operating with overall suspended, retained and attached particle concentrations are used in the current work for fines migration prediction and assessment.

Other temperature-sensitive rock parameters affecting geothermal exploration and production are porosity, electrical conductivity and seismic properties (Jaya et al., 2010; Kristinsdottir et al., 2010; Milsch et al., 2010; Rosenbrand et al., 2015).

The most commonly used approach for evaluating fines migration, retention and detachment in laboratory and field-scale studies is to apply the mass balance equation for solute transport with the sink term for particle retention and the source term for particle dislodging (Schijven and Hassanizadeh, 2000; Logan, 2001; Cortis et al., 2006; Tufenkji, 2007; Shapiro and Yuan, 2013):

$$\frac{\partial}{\partial t}(\phi c + \sigma) + U\frac{\partial c}{\partial x} = D\frac{\partial^2 c}{\partial x^2} \quad (1)$$

$$\frac{\partial \sigma}{\partial t} = \lambda(\sigma) c U - k_{\mathrm{det}}\sigma \quad (2)$$

where c and σ are dimensionless volumetric concentrations of suspended and strained particles, respectively; U is the flow velocity and D is the diffusion coefficient.

The capture term in Eq. (2) is proportional to the advective particle flux; the proportionality coefficient λ is called the filtration coefficient. The detachment term is proportional to the retained concentration; the proportionality coefficient k_{det} is called the

* Corresponding author.
E-mail address: zyou@asp.adelaide.edu.au (Z. You).

http://dx.doi.org/10.1016/j.geothermics.2015.05.008
0375-6505/

Nomenclature

C_v	coefficient of variance
c	volumetric concentration of suspended particles
D	diffusion coefficient ($L^2 T^{-1}$)
F	force ($M L T^{-2}$)
i	index
j	index
k	permeability (L^2)
k_{det}	detachment rate coefficient (T^{-1})
L	length of core (L)
l	lever (L)
n	index
p	pressure ($M T^{-2} L^{-1}$)
Q	intermediate function
r	radius (L)
S	dimensionless concentration of retained particles
T	temperature (K)
t	time (T)
U	Darcy velocity ($L T^{-1}$)
x	distance (L)

Greek letters

α	drift delay factor
β	formation damage coefficient
γ	ionic strength
ε	erosion ratio (ratio between the torques of detaching and attaching forces)
λ	filtration coefficient (L^{-1})
μ	dynamic viscosity ($M L^{-1} T^{-1}$)
Σ	concentration distribution of captured particles (L^{-1})
σ	volumetric concentration of captured particles
ϕ	porosity

Subscripts

a	attachment
cr	critical (for the maximum retention function)
D	dimensionless
d	drag
e	drainage (for reservoir radius), electrostatic (for force)
g	gravitational
l	lifting
s	straining (for retained concentration), radius (for particles)
scr	critical radius (for retained particles)
0	initial value

detachment rate coefficient. System of Eqs. (1) and (2) together with the micro-scale-modelling-based formula for coefficient λ is called the classical filtration theory in the above references. The advanced theory for the filtration coefficient dependency on particle–grain and particle–particle interactions, flow velocity, Brownian diffusion and gravitational sedimentation has been developed (Nabzar and Chauveteau, 1997; Chauveteau et al., 1998; Tufenkji and Elimelech, 2004; Rousseau et al., 2008; Yuan and Shapiro, 2012), while the detachment coefficient is an empirical constant usually determined by tuning from the experimental data. This is a shortcoming of the advective-diffusive attachment–detachment model with kinetics of the particle detachment ((1) and (2)).

Another shortcoming is the asymptotic stabilisation of the retention concentration and permeability when time tends to infinity, while the fines release due to abrupt pressure gradient

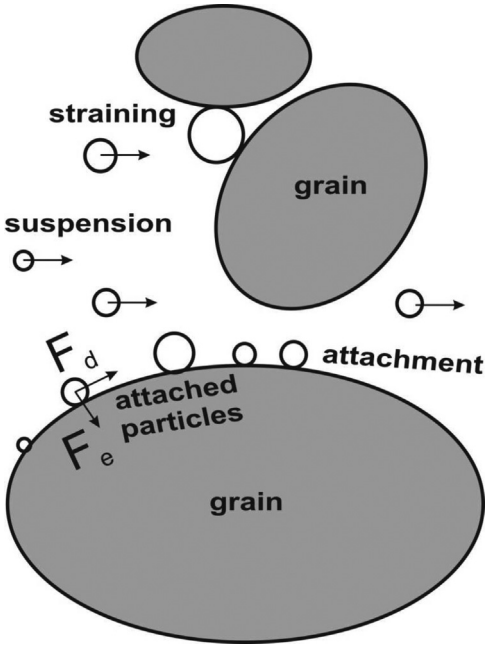

Fig. 1. Fines mobilisation, migration and straining in porous media (F_d: drag force, F_e: electrostatic force).

increase or under salinity alternation happens almost instantly (Miranda and Underdown, 1993; Khilar and Fogler, 1998). The coreflood with sharp rate increase shows an immediate permeability response (Ochi and Vernoux, 1998; Bedrikovetsky et al., 2012; Oliveira et al., 2014).

It has long been recognised that the particle detachment happens if the mechanical equilibrium of a retained particle on the internal filter cake does not take place (Schechter, 1992; Rahman et al., 1994; Civan, 2007). The forces acting on a particle placed on the internal cake are: electrostatic, drag, lifting and gravitational forces. In the majority of the cases, lifting and gravitational forces can be neglected. In particular, the analyses under both ambient and geothermal reservoir conditions show that gravitational and lifting forces are negligible if compared with electrostatic and drag forces (You et al., 2014). Therefore, only drag and electrostatic forces are shown in Fig. 1. Some authors consider a force balance between the drag force acting on the particle from the by-passing fluid, and the friction force with an empirical Coulomb coefficient (Civan, 2007). Another approach includes the momentum balance of forces (Jiao and Sharma, 1994; Freitas and Sharma, 2001):

$$F_d(U, T, r_s)l(r_s) = F_e(\gamma, T, r_s), \quad l = \frac{l_d}{l_e} \tag{3}$$

where F_d and F_e are drag and electrostatic forces, respectively, l_d and l_e are corresponding lever arms, l is the lever arm ratio, U is flow velocity, γ is the ionic strength of the reservoir brine and r_s is the particle radius.

The modified Stokes' formula is derived for a spherical particle located on at the pore wall, and expresses the drag force via velocity and the particle radius (Jiao and Sharma, 1994; Ochi and Vernoux, 1998; Bradford et al., 2013). The drag force expression contains the shape factor that accounts for the particle form, its deformation on the rock surface by attractive electrostatic forces and the rock surface roughness.

Electrostatic force is calculated from the total interaction potential energy. At the micron scale of the reservoir fines, this energy is the sum of London-van-der-Waals, electrical double layer and Born potentials. The explicit expressions of three interaction potential energies are given by the DLVO

Please cite this article in press as: You, Z., et al., Mathematical modelling of fines migration in geothermal reservoirs. Geothermics (2015), http://dx.doi.org/10.1016/j.geothermics.2015.05.008

(Derjaguin–Landau–Verwey–Overbeek) theory (Derjaguin and Landau, 1941; Verwey and Overbeek, 1948; Israelachvili, 2011). The explicit formulae for the three respective forces versus water ionic strength, velocity, particle and pore radii, as applied for fines migration and used further in this paper, can be found from Khilar and Fogler (1998).

The two approaches are mathematically equivalent. The advective-diffusion equation with kinetic detachment term ((1) and (2)) does not reflect the particle mechanical equilibrium; the detachment term is not affected by the mechanical equilibrium of a single particle.

Drag force in Eq. (3) depends on velocity and particle radius while electrostatic force depends on particle radius, ionic strength and temperature. It allows expressing particle radius r_s from transcendental Eq. (3): $r_{scr} = R(U, \gamma, T)$. For the above mentioned expressions for drag and electrostatic forces, the function R monotonically decreases with U and T, and monotonically increases with γ. It means that r_{scr} is the minimum size of particles mobilised by flow during increase of fluid velocity and temperature, and decrease of salinity, i.e. particles are removed in the order of their radii decrease. Therefore, the total remaining particle concentration is the sum of concentrations for all particles smaller than r_{scr}:

$$\sigma_a = \sigma_{cr}(U, \gamma, T), \quad \sigma_{cr}(U, \gamma, T) = \int_0^{r_{scr}(U,\gamma,T)} \Sigma_a(r_s) dr_s \tag{4}$$

where $\Sigma_a(r_s)$ is the size distribution of attached fine particles. The dependency (4) is called the maximum retention function. It is an empirical function of the properties of porous media and the flowing-through particles.

The modified mathematical model which models the particle release uses the maximum retention concentration as an instant function of velocity, salinity and temperature (Bedrikovetsky et al., 2011, 2012). Change of any of these three parameters at point (x, t) results in either increase or decrease of the maximum retention function, yielding either timely attachment of new particles to the rock or instant detachment. For flow regimes where velocity and temperature monotonically increase and salinity monotonically decreases, the maximum retention function decreases, and the attached particles are mobilised.

So, the maximum retention function is determined by the torque balance on the pore surface of the internal cake, Eq. (3). The phenomenological function (4) substitutes the particle release kinetics in the classical attachment–detachment model (2). The modified model (3) and (4) is free of the above mentioned shortcomings.

The maximum retention function is analogous to adsorption isotherm. The difference is the dependency of the maximum retention function on velocity, which is not a thermodynamic parameter (Bedrikovetsky, 1993). Maximum retention dependency (4) does not correspond to energy minimum, since the drag force in Eq. (3) does not have potential. However, Eq. (4) can be generalised as similar to non-equilibrium sorption.

The works by Bradford et al. (2012, 2013) account for kinetics of the particle release due to salt diffusion from the contact area between the particle and matrix surface, both deformed by the electrostatic "particle-rock" attraction. Their models correspond to the introduction of timely delay into the maximum retention function (4).

The conventional model ((1) and (2)) assumes that the mobilised particle speed is equal to the carrier fluid velocity. This assumption along with that of an instant particle release leads to zero outlet concentration after one pore volume injection, since the particle mobilised at the core entrance arrives at the outlet at the moment of one pore volume injected. Therefore, the pressure drop along the core also stabilises after injection of one pore volume. However, numerous laboratory studies show significant delay in pressure drop/permeability stabilisation (Lever and Dawe, 1984; Ochi and Vernoux, 1998; You et al., 2014). It is explained by slow particle drift near the grain surfaces (You et al., 2014). Slow movement of released particles have been noticed in several works. Sefrioui et al. (2013) investigated slow particle movement near to pore wall asperities using the Navier–Stokes-based micro-scale modelling. Yuan and Shapiro (2011) and Bradford et al. (2013) observed delayed particle arrival from the breakthrough concentration curves. They proposed the two-speed model that successfully matches the breakthrough concentrations. However, the model contains six empirical kinetics coefficients of mass transfer between attached, slow-near-wall and fast-in-bulk-water particles, which cannot be determined solely from the breakthrough concentration history. Significantly more sophisticated laboratory tests should be performed for complete characterisation of the two-speed model. Besides, mass exchange between fast and slow particle fluxes occurs on the pore scale, so the particle concentrations may be equal on the core scale causing propagation of the overall particle ensemble with the low average speed. Therefore, in the current work we use the single-velocity model with particle speed that is lower than the water velocity.

In the present paper, water flow velocity U in basic equations ((1) and (2)) is substituted by the particle velocity $U_s < U$ that explains long periods for permeability stabilisation by slow surface motion of the mobilised fine particles. Another modification of the governing system ((1) and (2)) is the introduction of the maximum retention function for a monolayer of size-distributed fines, allowing explaining its non-convex form. The exact solution to the obtained system of equations for one-dimensional flow with piecewise constant velocity increase is obtained. The laboratory data on pressure drop along the core during injection have been matched by the analytical model. It is shown that the mobilised particle speed is significantly lower than the carrier water velocity, i.e. $U_s \ll U$. Good agreement between the laboratory and modelling data validates the proposed model for a slow surface motion of released fine particles in porous media. Application of the laboratory-based model to fines migration at higher temperatures in geothermal reservoirs yields significantly higher permeability damage, compared with applications at conventional reservoir temperatures.

The present work uses the laboratory study data obtained in the companion paper by You et al. (2014).

The structure of the text is as follows. Section 2 presents the basic governing equations for one-dimensional suspension-colloidal transport with particle release, migration and straining along with analytical model for injection with piecewise constantly decreasing ionic strength. Tuning of the model coefficients from the laboratory data from the companion paper by You et al. (2014) is shown in Section 3. The discussions of the model validity conclude the paper.

2. Mathematical model for fines migration during coreflooding

In this section we present the model assumptions (Section 2.1), governing system of equations (Section 2.2) and its analytical solution (Section 2.3) for suspension flow with slow migration of detached fines and further straining. The derived analytical model is applied to experimental data treatment in Section 3.

2.1. Assumptions

The assumption that the particle velocity is equal to the carrier fluid velocity in (1) and (2) corresponds to permeability stabilisation at the moment $t = 1$ PVI. However, the laboratory data presented in Fig. 2(a) shows that even 25 PVI of the constant fluid ionic strength injection is not enough for the average permeability stabilisation. The delayed stabilisation effect can be explained

Please cite this article in press as: You, Z., et al., Mathematical modelling of fines migration in geothermal reservoirs. Geothermics (2015), http://dx.doi.org/10.1016/j.geothermics.2015.05.008

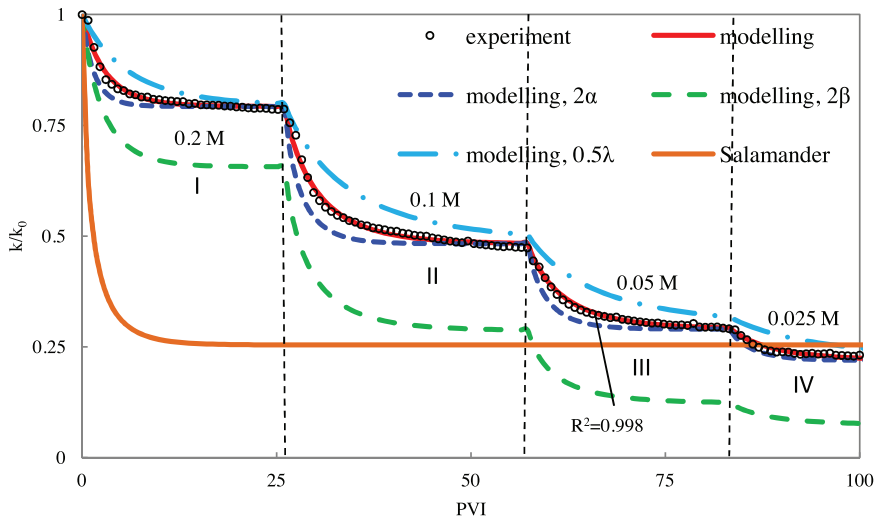

(a)

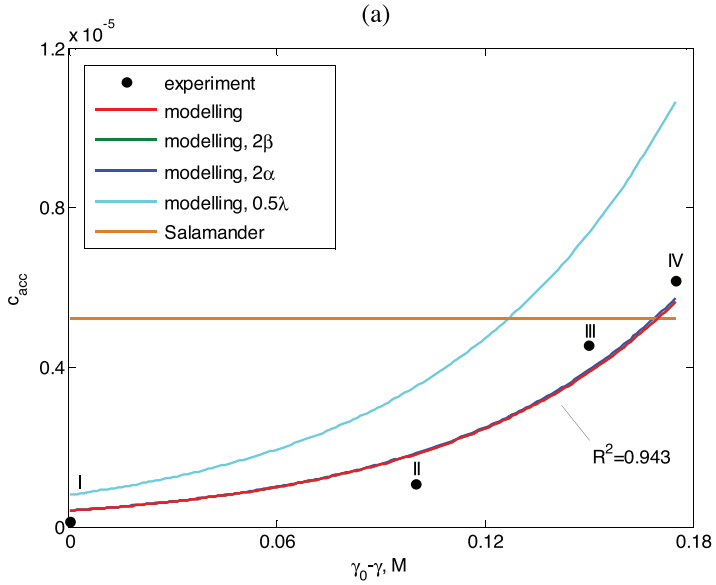

(b)

Fig. 2. Tuning the laboratory data from ionic strength alteration test at $T = 25\,^{\circ}C$ by the analytical model and prediction for Salamander geothermal field ($T = 129\,^{\circ}C$): (a) permeability decline of the core during coreflood with piecewise decreasing ionic strength; (b) cumulative breakthrough concentration (c_{acc}) at different ionic strength values (k: permeability, α: drift delay factor, β: formation damage coefficient, λ: filtration coefficient, γ: ionic strength). (For interpretation of the references to color in text near the figure citation, the reader is referred to the web version of this article.)

by slow drift of mobilised fines along the pore walls and stagnant zones, and also by particle sliding and rolling along the rock surface (Jiao and Sharma, 1994; Sefrioui et al., 2013). Therefore, below it is assumed that the particle transport velocity is equal to αU, where $\alpha < 1$.

The main assumptions of the mathematical model for fines mobilisation, migration and straining are:

- incompressible fluid and particles;
- volume additivity for fluid with suspended, attached and strained particles;
- constant porosity for low attached and strained concentrations;
- particle migration velocity different from the carrier fluid velocity;
- negligible dispersion of fine particles if compared with their advection;
- instant release of attached particles fulfilling the maximum retention condition (3) and (4);
- linear kinetics of the particle straining by porous media with constant filtration and formation damage coefficients;
- no strained particles in rocks before fines mobilisation;
- no detachment of strained particles; and
- negligible permeability increase due to particle detachment if compared with the permeability decrease due to particle straining.

Based on the above assumptions, the next section derives transport equations for colloids and suspensions accounting for particle release, migration and straining.

2.2. Governing equations

The mass balance equation for suspended, attached and strained fines in porous media is:

$$\frac{\partial(\phi c + \sigma_s + \sigma_a)}{\partial t} + \alpha U \frac{\partial c}{\partial x} = 0 \tag{5}$$

where σ_a and σ_s are concentrations of attached and strained fines. The drift delay factor α accounts for slow particle motion.

Please cite this article in press as: You, Z., et al., Mathematical modelling of fines migration in geothermal reservoirs. Geothermics (2015), http://dx.doi.org/10.1016/j.geothermics.2015.05.008

Particle straining rate is proportional to the suspension flux, delivering particles to pores with the throats smaller than the particles (Herzig et al., 1970):

$$\frac{\partial \sigma_s}{\partial t} = \lambda \alpha U c \tag{6}$$

The proportionality coefficient λ, which is called the filtration coefficient, is equal to the particle capture probability per unit length of the particle trajectory.

Darcy equation accounts for permeability decline due to size exclusion of fine particles:

$$U = -\frac{k(\sigma_s)}{\mu}\frac{\partial p}{\partial x}, \quad k(\sigma_s) = \frac{k_0}{1+\beta\sigma_s} \tag{7}$$

where k is the permeability as a function of strained particle concentration, β is the formation damage coefficient, k_0 is the initial permeability, μ is the viscosity of suspension and p is the pressure. The above expression for $k(\sigma_s)$ corresponds to the zero and first order Taylor expansion terms.

In the case of clean water injection into the core without initially strained fines, initial and boundary conditions are:

$$c(x,0) = 0, \quad c(0,t) = 0, \quad \sigma_a(x,0) = \sigma_{a0}, \quad \sigma_s(x,0) = 0 \tag{8}$$

The path $I \to A \to B \to C$ in Fig. 3(a) corresponds to initial and boundary conditions (8), i.e. to the transition occurring during the injection of water with ionic strength γ_2 into the core with water ionic strength γ_1. The diagram illustrates the ionic strength dependency of the attached particle concentration (see Eqs. (3) and (4)). Here, point $I(0, \sigma_{a0})$ corresponds to initial attached particle concentration. The attached particle concentration is given by the maximum retention function (3) and (4). The interval $I \to A$ corresponds to injection of water with the decreasing ionic strength without particle release. Further transition $A \to B$ ends up in release of the first particle with the injection of water with ionic strength γ_2. Further ionic strength decrease down to γ_3 yields the release of attached particles with the amount $\Delta\sigma$, which is instantly suspended in the flowing water with concentration $\Delta\sigma/\phi$.

Let us consider sequential injections of water with ionic strength $\gamma_i (i = 1, 2 \cdots)$. The suspended fines concentration due to particle release with ionic strength alteration from γ_{i-1} (during stage $i-1$) to γ_i (during stage i) can be calculated from the variation of attached concentration:

$$\Delta c(x,t_i) = \phi^{-1}\{\sigma_{cr}[\gamma(x,t_{i-1})] - \sigma_{cr}[\gamma(x,t_i)]\} = \phi^{-1}\Delta\sigma_a(\gamma_{i-1},\gamma_i) \tag{9}$$

i.e. the initial suspended concentration after ionic strength alteration becomes $\Delta\sigma/\phi$. In Eq. (9), t_i corresponds to the moment of ionic strength alteration from γ_{i-1} to γ_i.

The amount of released particles $\Delta\sigma$ in Fig. 3(a) represents the difference between the values of the maximum retention function corresponding to ionic strengths from γ_{i-1} to γ_i. Eq. (9) implies that all mobilised particles are instantly removed into suspension.

Since the attaching electrostatic force depends on water ionic strength, different sized particles are mobilised at different stages, so the values of the drift delay factor $\alpha_i = (i = 1, 2, \cdots)$ also change from stage to stage. The same relates to filtration and formation damage coefficients.

Introduce the following dimensionless variables into the governing system ((3) and (5)–(8)):

$$S_a = \frac{\sigma_a}{\phi}, S_s = \frac{\sigma_s}{\phi}, \lambda_D = \lambda L, t_D = \frac{1}{\phi L}\int_0^t U(y)dy, x_D = \frac{x}{L}, \alpha = \frac{U_s}{U} \tag{10}$$

where L is the core length and t_D is the injected water volume expressed in core pore volumes.

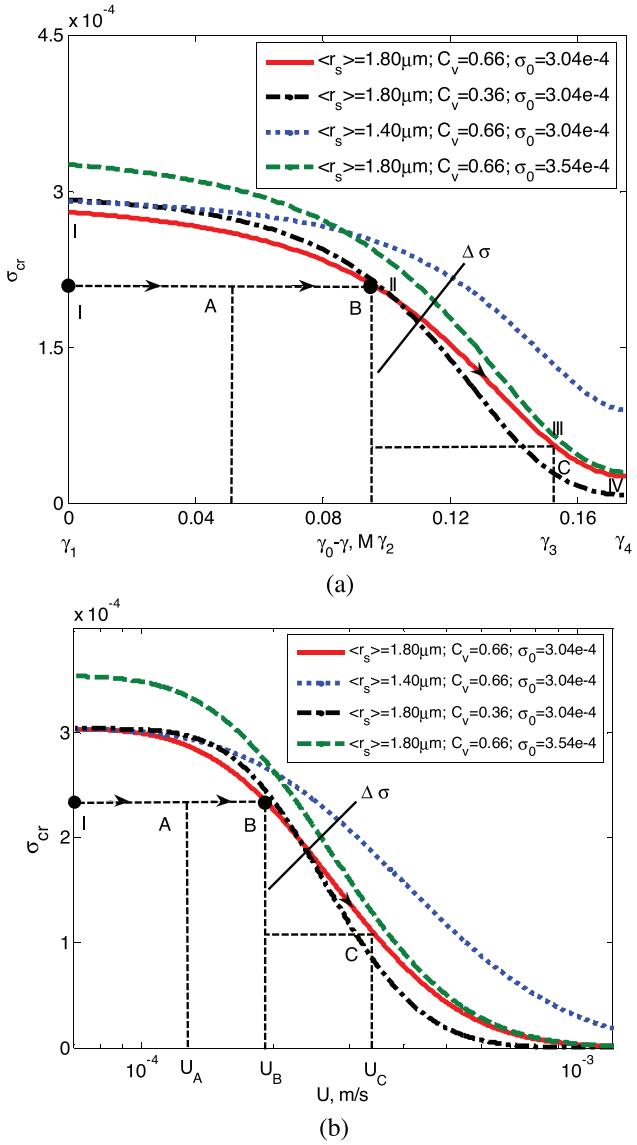

Fig. 3. The maximum retention concentration at different particle size distribution and maximum concentration value with: (a) ionic strength dependency, ionic strength values γ_1–γ_4 correspond to four conditions applied in the laboratory test, γ_0 = 0.2 M NaCl; (b) velocity dependency (σ_{cr}: maximum retention concentration, U: velocity, $\langle r_s \rangle$: mean particle size, C_v: variance coefficient, σ_0: initial concentration of attached particles). (For interpretation of the references to color in text near the figure citation, the reader is referred to the web version of this article.)

The dimensionless equations for the unknown suspended, strained and attached concentrations c_i, S_{si} and S_{ai} during stage i are obtained by substituting (10) into ((3) and (5)–(8)):

$$\frac{\partial(c_i + S_{si})}{\partial t_D} + \alpha_i \frac{\partial c_i}{\partial x_D} = 0 \tag{11}$$

$$\frac{\partial S_{si}}{\partial t_D} = \alpha_i \lambda_{Di} c_i \tag{12}$$

$$S_{ai}(x_D, t_D) = S_{cr}(\gamma_i) \tag{13}$$

$$c_i(x_D, t_{Di}) = c_{i-1}(x_D, t_{Di}) + \Delta S_a(\gamma_{i-1}, \gamma_i), \quad c_i(0, t_D) = 0, \quad S_{si}(x_D, t_{Di}) = S_{s,i-1}(x_D, t_{Di}) \tag{14}$$

The initial condition for c_i (the first equation in (14)) shows that the amount of particles, released at the moment t_{Di} when the

Please cite this article in press as: You, Z., et al., Mathematical modelling of fines migration in geothermal reservoirs. Geothermics (2015), http://dx.doi.org/10.1016/j.geothermics.2015.05.008

Table 1
Analytical model for fines mobilisation, migration and suspension.

Term	Notation	Expression
Suspended concentration during stage 1	$c_1(x_D, t_D)$	$\begin{cases} 0, & x_D \le \alpha_1(t_D - t_{D1}) \\ \Delta S_a(\gamma_0, \gamma_1) e^{-\alpha_1 \lambda_{D1}(t_D - t_{D1})} & x_D > \alpha_1(t_D - t_{D1}) \end{cases}$
Strained concentration during stage 1	$S_{s1}(x_D, t_D)$	$\begin{cases} \Delta S_a(\gamma_0, \gamma_1)(1 - e^{-\lambda_{D1} x_D}), & x_D \le \alpha_1(t_D - t_{D1}) \\ \Delta S_a(\gamma_0, \gamma_1)(1 - e^{-\alpha_1 \lambda_{D1}(t_D - t_{D1})}), & x_D > \alpha_i(t_D - t_{D1}) \end{cases}$
Permeability during stage 1	$k_1(t_D)$	$\frac{k_0}{1+\beta_1 \phi \int_0^1 S_{s1}(x_D, t_D) dx_D}$
Total suspended concentration during stage $i-1$	$\int_0^1 c_{i-1}(x_D, t_{Di}) dx_D$	$\sum_{j=2}^{i} \left[(x_{D(i-1),j} - x_{D(i-1),j-1}) \Delta S_a(\gamma_{i-j}, \gamma_{i-j+1}) \prod_{n=i-j+1}^{i-1} Q_n \right]$
Cumulative breakthrough concentration during stage i	$\int_{t_{Di}}^{t_D} \alpha_i c_i(1, t_D) dt_D$	$\frac{1}{\lambda_{Di}} \{1 - \exp[-\alpha_i \lambda_{D_i}(t_D - t_{Di})]\} \times \left\{ \Delta S_a(\gamma_{i-1}, \gamma_i) + \sum_{j=3}^{i+1} \left[\Delta S_a(\gamma_{i-j+1}, \gamma_{i-j+2}) \prod_{n=i-j+2}^{i-1} Q_n \right] \right\}$
Total suspended concentration during stage i	$\int_0^1 c_i(x_D, t_D) dx_D$	$\sum_{j=2}^{i+1} \left[(x_{Di,j} - x_{Di,j-1}) \Delta S_a(\gamma_{i-j+1}, \gamma_{i-j+2}) \prod_{n=i-j+2}^{i} Q_n \right]$
Total strained concentration during stage i	$\int_0^1 [S_{si}(x_D, t_D) - S_{s,i-1}(x_D, t_{Di})] dx_D$	$\Delta S_a(\gamma_{i-1}, \gamma_i) + \int_0^1 c_{i-1}(x_D, t_{Di}) dx_D - \left[\int_{t_{Di}}^{t_D} \alpha_i c_i(1, t_D) dt_D + \int_0^1 c_i(x_D, t_D) dx_D \right]$
Permeability during stage i	$k_i(t_D)$	$k_0 \left\{ \prod_{n=1}^{i} \left[1 + \beta_n \phi \int_0^1 (S_{sn}(x_D, t_D) - S_{s,n-1}(x_D, t_{Dn})) dx_D \right] \right\}^{-1}$

salinity switches from γ_{i-1} to γ_i, adds to the suspended concentration profile inherited from the injection of water with salinity γ_{i-1}.

System of four equations (7) and (11)–(13) subject to initial and boundary conditions (14) determines unknown suspended, attached and strained concentrations along with pressure during stage i. The system for concentrations (11)–(13) separates from Eq. (7) for pressure, i.e., the pressure is determined from Eq. (7) after the solution of system (11)–(13).

2.3. Analytical solution

Instant particle release with the following migration and straining is a linear hyperbolic problem allowing for exact solution. The explicit expressions for suspended and strained concentrations along with pressure drop across the core have been presented for the previously discussed case of $\alpha = 1$ (Bedrikovetsky et al., 2011, 2012). The derivations of the analytical model for $\alpha < 1$ are briefly presented in this section.

Suspended fines concentration is determined from Eqs. (11) and (12) using the method of characteristics (Tikhonov and Samarskii, 2013):

$$c_i(x_D, t_D) = \begin{cases} 0, & x_D \le \alpha_i(t_D - t_{Di}) \\ [c_{i-1}(x_D, t_{Di}) + \Delta S_a(\gamma_{i-1}, \gamma_i)] e^{-\alpha_i \lambda_{Di}(t_D - t_{Di})}, & x_D > \alpha_i(t_D - t_{Di}) \end{cases} \quad (15)$$

where $\alpha_i = dx_D/dt_D$ is the speed of the concentration front (Fig. 4(a) shows the first stage). Substituting (15) into straining rate equation (12) and integrating over time result in the formula for strained concentration (the second row in Table 1 shows the strained concentration for the first stage S_{s1}). The suspended concentration is equal to zero behind the front. The moment $1/\alpha_1$ corresponds to the arrival of the "last" released fine particle at the core outlet. Fig. 4(b) shows the three suspended concentration profiles at $t_D = 0$, at the moment t_{Da} before the front arrival at the core outlet and at the moment t_{Db} after the front arrival. The initial suspended concentration is ΔS_{a1}. Before the front arrival, the suspended concentration is equal to zero behind the front and is constant ahead of the front. This constant decreases with time; see (15). The suspended concentration becomes zero after the front arrival, since all particles become either strained or produced at the outlet. Three profiles of strained concentration at moments 0, t_{Da} and t_{Db} are demonstrated in Fig. 4(c). There are no strained particles in rocks before fines mobilisation. The strained concentration grows with time until the front arrival and remains constant afterwards. The larger is the x_D, the longer is the stabilisation time and the higher is the maximum value of accumulated strained particles, therefore the strained profile grows as x_D increases. The profile is uniform ahead of the front since the particle advective flux is uniform and the particle capture probability is constant.

Suspended fines concentration during stage i is the sum of concentrations of particles inherited from all the previous stages by applying Eq. (15) to each stage:

$$c_{i,j}(x_D, t_D) = \begin{cases} 0, & j = 1 \\ \sum_{j=2}^{i+1} \left(\Delta S_a(\gamma_{i-j+1}, \gamma_{i-j+2}) \prod_{n=i-j+2}^{i} Q_n \right) & j > 1 \end{cases} \quad (16)$$

in which the function Q_n is defined as

$$Q_n(t_D) = e^{-\alpha_n \lambda_{Dn}(t_D - t_{Dn})} \quad (17)$$

As it follows from the particle population balance equation (11), the total strained concentration in porous media is equal to the initial suspended and strained concentrations at the beginning of stage i minus the total concentration of breakthrough particles and particles suspended in the core. Therefore, the total strained concentration is obtained as:

$$\int_0^1 S_{si}(x_D, t_D) dx_D = \underbrace{\Delta S_a(\gamma_{i-1}, \gamma_i) + \int_0^1 c_{i-1}(x_D, t_{Di}) dx_D + \int_0^1 S_{s,i-1}(x_D, t_{Di}) dx_D}_{initial\ \ particles} - \left[\underbrace{\int_{t_{Di}}^{t_D} \alpha_i c_i(1, t_D) dt_D}_{breakthrough\ particles} + \underbrace{\int_0^1 c_i(x_D, t_D) dx_D}_{suspended\ \ particles} \right] \quad (18)$$

Please cite this article in press as: You, Z., et al., Mathematical modelling of fines migration in geothermal reservoirs. Geothermics (2015), http://dx.doi.org/10.1016/j.geothermics.2015.05.008

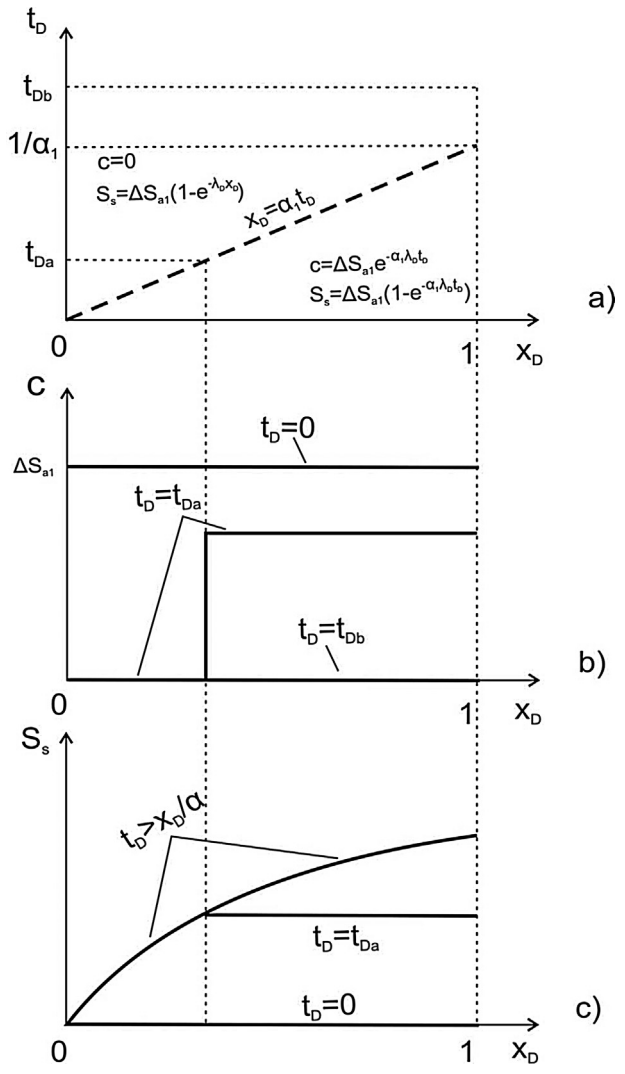

Fig. 4. Solution of fines migration problem under elevated velocity: (a) trajectory of fronts and characteristic lines in (x_D, t_D) plane; (b) suspended concentration profiles in three moments; (c) strained concentration profiles in three moments (c: concentration of suspended particles, S_s: concentration of strained particles, α: drift delay factor, λ: filtration coefficient).

where

$$\int_0^1 c_{i-1}(x_D, t_{Di})dx_D = \sum_{j=2}^{i}\left[(x_{D(i-1),j} - x_{D(i-1),j-1})\Delta S_a(\gamma_{i-j}, \gamma_{i-j+1})\prod_{n=i-j+1}^{i-1} Q_n\right] \quad (19)$$

represents the total suspended concentration along the core at the end of stage $i-1$. This term together with the mobilised particle concentration at the beginning of stage i provides the total initial suspended concentration for stage i. The cumulative breakthrough concentration during stage i and the total suspended concentration along the core during stage i are obtained by substituting Eq. (16) into the last two terms of (18):

$$\int_{t_{Di}}^{t_D} \alpha_i c_i(1, t_D)dt_D = \frac{1}{\lambda_{Di}}\left\{1 - \exp[-\alpha_i\lambda_{D_i}(t_D - t_{Di})]\right\}\left\{\Delta S_a(\gamma_{i-1}, \gamma_i) + \sum_{j=3}^{i+1}\left[\Delta S_a(\gamma_{i-j+1}, \gamma_{i-j+2})\prod_{n=i-j+2}^{i-1} Q_n\right]\right\} \quad (20)$$

$$\int_0^1 c_i(x_D, t_D)dx_D = \sum_{j=2}^{i+1}\left[(x_{Di,j} - x_{Di,j-1})\Delta S_a(\gamma_{i-j+1}, \gamma_{i-j+2})\prod_{n=i-j+2}^{i} Q_n\right] \quad (21)$$

The permeability as a function of time during stage i is expressed from the second equation of (7), accounting for permeability decline history at each stage:

$$k_i(t_D) = k_{i-1}\{1 + \beta_i\phi\int_0^1 [S_{si}(x_D, t_D) - S_{s,i-1}(x_D, t_{Di})]dx_D\}^{-1} = k_0\left\{\prod_{n=1}^{i}[1 + \beta_n\phi\int_0^1 (S_{sn}(x_D, t_D) - S_{s,n-1}(x_D, t_{Dn}))dx_D]\right\}^{-1} \quad (22)$$

where $\int_0^1 [S_{si}(x_D, t_D) - S_{s,i-1}(x_D, t_{Di})]dx_D$ is the total strained concentration along the core during stage i, calculated from Eq. (18).

The formulae in the analytical model are summarised in Table 1. The suspended concentration during stage 1 is c_1, as obtained from Eq. (15) by letting $i = 1$ (see the first row in Table 1). Substituting c_1 into Eq. (12) and integrating over t_D result in strained concentration S_{s1} at stage 1 (see the second row in Table 1). Permeability k_1 during stage 1 is then calculated from (22) and listed in the third row of Table 1. Integrating suspended concentration at the end of the previous stage $i-1$ over the core length $\int_0^1 c_{i-1}(x_D, t_{Di})dx_D$ delivers the total suspended concentration inherited from stage $i-1$ (the fourth row in Table 1). Cumulative breakthrough concentration during stage i is obtained from Eq. (20) as $\int_{t_{Di}}^{t_D} \alpha_i c_i(1, t_D)dt_D$ (the fifth row in Table 1). The total suspended concentration during stage i is calculated from Eq. (21) as $\int_0^1 c_i(x_D, t_D)dx_D$ (the sixth row in Table 1). The seventh row in Table 1 presents the total strained concentration during stage i, $\int_0^1 [S_{si}(x_D, t_D) - S_{s,i-1}(x_D, t_{Di})]dx_D$, resulting from Eq. (18). Permeability k_i during stage i is calculated from (22) and listed in the last row of Table 1.

3. Treatment of experimental data

The analytical model presented in Section 2.3 is applied to the treatment of experimental data obtained from the coreflood test with piecewise decreasing ionic strength (see the paper by You et al. (2014) for details of the laboratory procedure). The core is taken from Ladbroke Grove formation, which has the rock properties analogous to that in Salamander geothermal field (Badalyan et al., 2014). The following experimental procedures have been applied to the sandstone core with porosity 17.2%, permeability 5.46 mD and length 6.33 cm:

- The core is evacuated down to 1.5 Pa and saturated with 0.6 M NaCl solution;
- The core is placed inside the high-pressure core holder with overburden pressure of 1000 psi;
- 0.6 M NaCl solution is pumped through the core with velocity of 1.4×10^{-4} m/s until the stabilisation of rock permeability, within experimental uncertainty, is reached;
- Effluent samples are collected, particle concentration and size distribution are measured by PAMAS S4031 GO portable particle counter (PAMAS GmbH, Salzuflen, Germany);

Table 2
Values of the model tuning parameters in the coreflood test.

Parameter	Value
r_s (μm)	1.80
C_v	0.66
σ_0	3.04e−4
α_1	4.10e−3
α_2	2.96e−3
α_3	2.81e−3
α_4	2.74e−3
β_1	9793
β_2	7631
β_3	7391
β_4	7158
λ_{D1}	67.14
λ_{D2}	53.79
λ_{D3}	51.11
λ_{D4}	50.13

- Ionic strength is decreased to 0.4 M NaCl and the above procedure is repeated;
- Coreflood tests are performed using water with ionic strengths 0.2, 0.1, 0.05 and 0.025 M NaCl.

The experimental data are presented in Fig. 2. The test started by injection of high salinity water with 0.6 M and 0.4 M NaCl, which is not shown in Fig. 2a. The permeability was observed to remain constant, defined as the initial permeability k_0. The experimental data of permeability decline history (black circles in Fig. 2(a)) and particle concentration at the outlet (black points in Fig. 2(b)) are used for model tuning. The lognormal form for the particle size distribution is assumed. The method for calculation of the maximum retention function for monolayer of size distributed particles is given by You et al. (2014). The method includes determination of the minimum particle radius r_{scr} mobilised by the injected water with ionic strength γ, from the torque balance equation. So, the particles smaller than r_{scr} remain attached to the rock surface. Therefore, the maximum retention concentration is the total concentration of initially attached particles with radii smaller than $r_{scr}(\gamma)$.

The tuning parameters are: mean particle size $\langle r_s \rangle$, variance coefficient for particle size distribution C_v, drift delay factor α, formation damage coefficient β and filtration coefficient λ. The lower is the injected ionic strength, the smaller particles are mobilised. We assume constant particle radius of mobilised fines at each stage. Therefore, the drift delay factor, formation damage coefficient and filtration coefficient are constant for each stage. Least square goal function of deviation between the model predicted and measured data is used in the model tuning procedure. The Levenberg–Marquardt minimisation algorithm has been applied (Marquardt, 1963). The obtained values of tuning parameters are listed in Table 2. The optimised permeability and outlet concentration curves from modelling are shown as red curves in Fig. 2(a) and (b), respectively. Good agreement is observed between the measured data and model prediction for both permeability and outlet concentration results (the coefficient of determination is $R^2 = 0.998$ for permeability data and $R^2 = 0.943$ for outlet concentration data), which validates the proposed model.

Sensitivity analysis with respect to the three main parameters in the model is presented in Fig. 2(a) and (b). Increase of the drift delay factor α decreases the stabilisation time due to faster movement of particles (see the blue dashed curve in Fig. 2(a)). The smaller filtration coefficient λ corresponds to lower particle capture probability, which leads to longer stabilisation time (light blue dash-dot curve in Fig. 2(a)). The larger formation damage coefficient β causes greater permeability decline over time (green dashed curve in Fig. 2(a)). Fig. 2(b) shows that only the filtration coefficient λ has significant effect on breakthrough particle concentration because it directly characterises the capture probability of released particles. Decrease of filtration coefficient λ yields higher breakthrough concentration (light blue curve). The effect of the drift delay factor α on breakthrough concentration is negligible, since the concentration of breakthrough particles is much lower than the released particle concentration $\Delta\sigma_i$ from the laboratory test, which means that the breakthrough concentration is insensitive to α (blue curve). Formation damage coefficient β does not affect the breakthrough concentration (green curve).

To address the uniqueness of the fitting parameters, we searched in 20% neighbourhood of the optimal point $\boldsymbol{x}_0$, $\boldsymbol{x}_0 = (\langle r_s \rangle, C_v, \alpha, \beta, \lambda)$, i.e. "initial guess points" for iterative minimisation were set as $1.1\boldsymbol{x}_0$ and $0.9\boldsymbol{x}_0$. So, 10 runs of the optimisation algorithm were performed. All runs converge to the point $\boldsymbol{x}_0$, i.e. the minimum is unique in its 20%-neighbourhood. The coefficient of determination R^2 is lower in all initial guess points than that at the optimal point. To conclude, the obtained optimum is unique in its 20%-neighbourhood. The most sensitive parameters with respect to permeability are the mean particle size $\langle r_s \rangle$ and formation damage coefficient β, while the breakthrough concentration is more sensitive to the filtration coefficient λ.

The orange curve corresponds to the geothermal temperature of the Salamander field; other curves are obtained based on the experimental data (Fig. 2).

The obtained values of filtration and formation damage coefficients (Table 2) are located inside the common intervals of these parameters (Nabzar and Chauveteau, 1997; Pang and Sharma, 1997; Sharma et al., 2000; Civan, 2007).

Fig. 3(a) presents the ionic strength dependency of the maximum retention concentration σ_{cr} calculated from the size distributed monolayer particle model. Red curve corresponds to the tuned values of mean radius and variance coefficient of the attached particle size distribution (Table 2). The maximum retention concentration decreases as ionic strength decreases.

Drag force exerting on fines is proportional to the square of particle size, while the particle-size dependency of electrostatic force is significantly weaker (Khilar and Fogler, 1998; Israelachvili, 2011). Therefore, $r_{scr}(\gamma)$ is a monotonically decreasing function and the particles are mobilised in decreasing order of their sizes with the decrease of ionic strength.

The smaller variance coefficient corresponds to the narrower size distribution of fines. The fraction of large particles is higher for curve with larger variance coefficient. Therefore, the smaller is the variance coefficient, the larger is the maximum retention concentration at high ionic strength (black dash-dot curve in Fig. 3(a)). The maximum retention concentration decreases as the variance coefficient decreases at low ionic strength.

The smaller mean particle size yields higher small particle fraction in the overall particle size distribution, resulting in higher maximum retention concentration (blue dotted curve). The higher σ_0 leads to the higher σ_{cr} at the given ionic strength (green dashed curve).

For the case of monolayer of size distributed attached particles, the size distribution function can be determined from the maximum retention function. Taking derivatives of both sides of Eq. (4) allows expressing the attached concentration distribution $\Sigma_a(r_s)$ via σ_{cr}. However, the resulting formula includes derivative of the experimentally determined function and, therefore, represents an ill-posed solution of the inverse problem (Tikhonov and Samarskii, 2013). Here, we determine a well-posed solution assuming lognormal size distribution for attached particles and define the mean particle size and standard deviation for this distribution by least-square fitting. Size distribution of attached particles obtained from the monolayer particle model is shown in Fig. 5. The fitted curve corresponds to the mean particle size 1.80 μm and the variance coefficient 0.66 (Table 2). Axis of abscissa presents the four

Please cite this article in press as: You, Z., et al., Mathematical modelling of fines migration in geothermal reservoirs. Geothermics (2015), http://dx.doi.org/10.1016/j.geothermics.2015.05.008

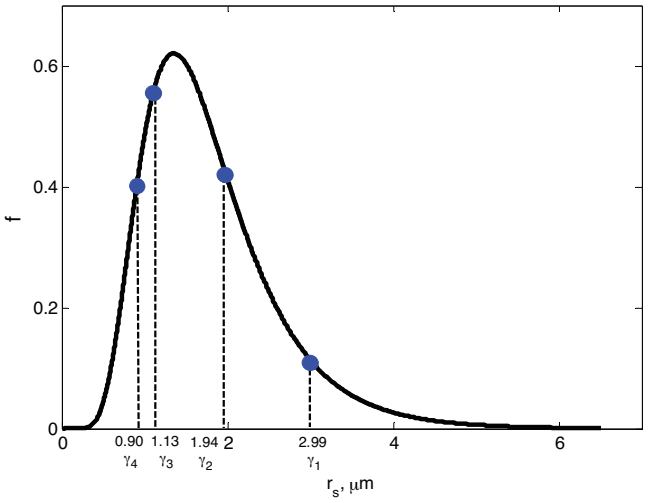

Fig. 5. Size distribution of movable particles obtained from the model (r_s: particle size, f: size distribution function, γ: ionic strength).

critical particle radii corresponding to the four ionic strength values $\gamma_1 \sim \gamma_4$ applied in the coreflood test with piecewise decreasing ionic strength. The critical size of mobilised fines decreases with the reduction of ionic strength from stage 1 to stage 4 (Fig. 5), resulting in the simultaneous decrease of drift delay factor α, formation damage coefficient β and filtration coefficient λ during the test (Table 2).

After calculation of the size distribution $\Sigma_a(r_s)$ for attached particles, we translate the maximum retention concentration as an ionic strength function $\sigma_{cr}(U_0, \gamma)$, into the velocity dependency of the maximum retention concentration $\sigma_{cr}(U_0, \gamma)$. The procedure is described in Section 2.3. The curve $\sigma_{cr}(U_0, \gamma)$ as obtained by the model fitting is shown in Fig. 3(a) in red; the translated curve $\sigma_{cr}(U_0, \gamma)$ is given in Fig. 3(b) in red as well.

The permeability impairment due to fines migration under different temperatures can be estimated by the second equation in (7) using the maximum retention function. Fig. 6 shows dimensionless permeability versus flow velocity (Fig. 6(a)) and ionic strength (Fig. 6(b)) during fines migration at different temperatures. The elevated temperature results in the reduction of electrostatic attaching force (Schembre and Kovscek (2005) have shown it for the conditions of steam-flooding in oilfields; Rosenbrand et al. (2012) reported this effect for kaolinite–quartz interaction in geothermal reservoirs); it also yields decrease of detaching forces due to reduction of fluid viscosity (García et al., 2006; Rosenbrand et al., 2015). Domination of the temperature effect on the electrostatic attaching force reduction leads to the maximum retention concentration as a decreasing function of temperature. Consequently, the higher is the temperature, the larger is the permeability decline during fines migration (Fig. 6(a) and (b)). Weakened electrostatic attaching force at geothermal reservoir temperature $T = 129\,^{\circ}C$ of the Salamander field and ionic strength γ below 0.2 M NaCl lead to nearly complete fines detachment (orange curve in Fig. 2(b)). Therefore, the maximum retention concentration approaches zero, causing the permeability reduction to a constant level throughout the range of $\gamma \leq 0.2$ M NaCl (orange curve in Fig. 2(a) and black dashed curve in Fig. 6(b)).

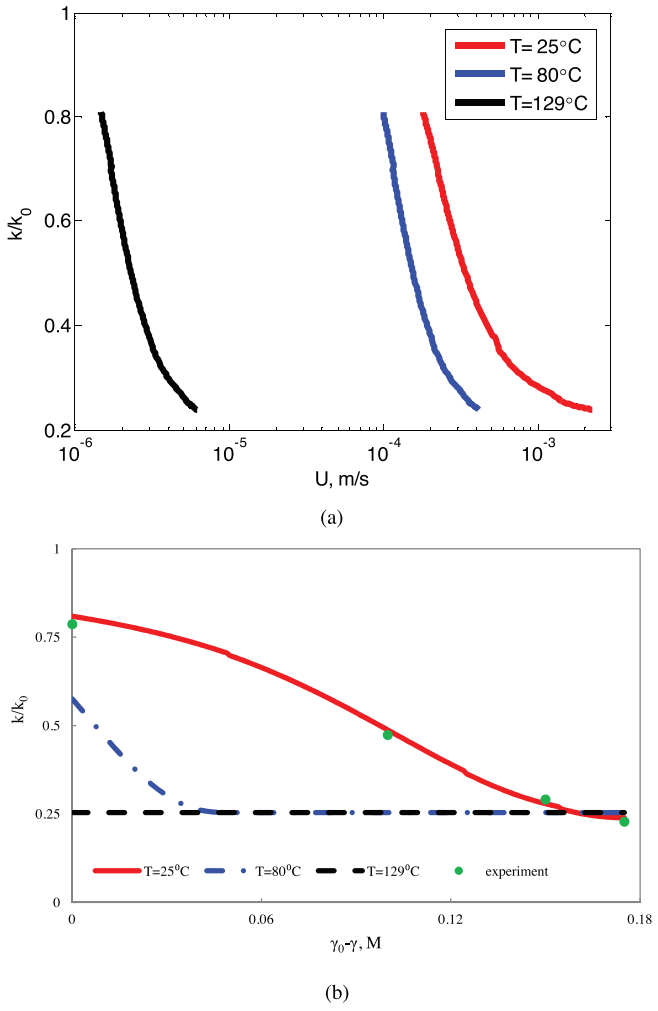

Fig. 6. Temperature effect on rock permeability due to fines migration: (a) velocity dependency; (b) ionic strength dependency (k: permeability, U: velocity, γ: ionic strength, T: temperature).

4. Discussions

The mathematical model derived in the present work has some limitations (see the assumptions in Section 2.1). The filtration and formation damage coefficients are considered to be constant, which corresponds to small retention concentration. For the case of high concentration of retained particles, the retention–concentration-dependent filtration and formation damage functions must be considered.

The laboratory data presented show an instant permeability response to abrupt ionic strength variation. The same phenomenon has been observed in several other studies (Ochi and Vernoux, 1998; Bedrikovetsky et al., 2012). However, some studies report the significant delay between the ionic strength alteration and fines mobilisation. It is explained by slow diffusion of the injected water into the contact area between the matrix surface and the fine particle, where both are deformed by attractive electrostatic force. It is important to understand which physical phenomena are responsible for the difference between two cases.

In the present work, the model for monolayer of size distributed attached fine particles has been considered. The previously derived equation for multilayers of mono sized particles has not been used in the present study, since it exhibits a convex form of the maximum retention function, while the experimental data indicate that the form is not convex (Fig. 3). However, both models are simplified versions of the multilayer of size distributed particles. Derivation of the maximum retention function for the latter case would enrich the mathematical model for fines migration in geothermal fields.

The two-speed model by Yuan and Shapiro (2011) and Bradford et al. (2012) describes particle detachment and transport in more details than the single velocity model, see Eqs. (11)–(13). In

Please cite this article in press as: You, Z., et al., Mathematical modelling of fines migration in geothermal reservoirs. Geothermics (2015), http://dx.doi.org/10.1016/j.geothermics.2015.05.008

reality, the model (11)–(13) is a particular case of the two-speed model, describing only the particles that drift near to pore walls and assuming zero concentration of the particles suspended in the bulk of carrier water. This case corresponds to low velocity of the carrier fluid, where the detaching force is not sufficient to deliver the mobilised particles into the bulk stream.

The two-speed model contains six kinetics coefficients of mass exchange between the attached particles, the slowly drifting particles near to pore walls and the fast moving particles transported within the bulk of carrier fluid. It is important to find out whether breakthrough concentration curve along with the pressure drop is enough to tune all the model parameters. If not, more sophisticated measurements should be performed: post-mortem measurements of retained profile using chemical analysis, "fast" CT-scanning as applied during the injection where the scanner moves along the core, measurements of pressure drop in the intermediate core points, suspension sampling in the intermediate ports, etc.

The effect of increased temperature on permeability reduction has been reported by several authors and is attributed mostly to fines mobilisation (Khilar and Fogler, 1998; Rosenbrand et al., 2014, 2015). See the detailed analysis of published experimental data in Rosenbrand and Fabricius (2012). These results support the conclusion of the present work that natural reservoirs with elevated temperatures are more susceptible to fines-migration-induced formation damage.

The analytical model shows that the temperature increase yields significant increase in the permeability impairment due to fines mobilisation, migration and subsequent size exclusion. As it follows from this statement, geothermal fields are more susceptible to fines migration with consequent well productivity impairment than conventional aquifers or oilfields. The phenomenon is explained by two competitive effects of temperature increase on fines mobilisation. On the one side, the increase in the reservoir temperature yields decrease of the maximum retention function due to the decrease of electrostatic attaching force. On the other side, the temperature increase also leads to the decrease of fluid viscosity, which results in the reduction of detaching drag and lifting forces, and resultantly, the maximum retention function increase. So, the maximum retention function is determined by these two competitive effects. Implementation of the laboratory-based temperature dependencies of electrostatic constant and water viscosity with corresponding modelling shows that the temperature effect on electrostatic constants dominates over the viscosity effect. Domination of the temperature effect on electrostatic attaching force results in the maximum retention function decrease and permeability reduction increase during the temperature rise. Therefore, the orange curve of permeability decline during fines mobilisation at elevated temperature of the Salamander geothermal field in Fig. 2(a) is located below the other curves, which are obtained at lower temperatures. Finally, the temperature increase from ambient conditions ($T = 25\,^{\circ}C$) to typical geothermal reservoir conditions ($T = 129\,^{\circ}C$) yields decrease in maximum retention function nearly to zero and consequent significant permeability decline.

The permeability-damage sensitivity to the physical parameters $\langle r_s \rangle$, C_v, β, λ and γ presented in Section 3, implies different production well behaviour in geothermal reservoirs with different rock and fluid properties. The rock permeability decline is greater for larger particles and higher formation damage coefficient. The larger is the jamming ratio (between mean particle and pore radii), the higher is the formation damage coefficient. The mean pore radius has the order of magnitude $(k/\phi)^{1/2}$. So, larger values of dimensionless group $r_s(k/\phi)^{-1/2}$ yield higher susceptibility of the reservoir to fines-migration-induced formation damage. The lower is the ionic strength of the reservoir brine, the smaller is the maximum retention concentration, the larger is the amount of mobilised fine particles and more severe is the formation damage in production wells.

The experimental procedure applied in the present study can be significantly improved. As it is concluded from the history matching of experimental data (Section 3), the rock permeability is sensitive mostly to mean particle size and formation damage coefficient, while the breakthrough concentration is most sensitive to filtration coefficient. The online measurements of particle concentration and size distribution in the effluent fluid enhance the accuracy of mean particle size and filtration coefficient estimation, while the computed tomography (CT) scan of the particle retention profile allows for more accurate determination of the formation damage coefficient (Mays and Hunt, 2005, 2007). However, in this case the population balance model must be used for the parameter tuning (Sharma and Yortsos, 1987a,b; Bedrikovetsky, 2008; Yuan et al., 2013).

5. Conclusions

Modification of the basic equations for fines migration by introducing the drift delay factor and a new form of maximum retention function for size-distributed fine particles, analytical modelling of one-dimensional flows and matching the laboratory coreflood data allow drawing the following conclusions:

- Analytical model for fines mobilisation, migration and straining yields the explicit formulae for suspended and strained concentrations, and permeability along the core;
- Large permeability stabilisation periods during fines migration can be explained by slow motion of released rolling or sliding particles; introduction of the drift delay factor allows for the permeability history matching;
- Good match between the laboratory measured and model predicted permeability has been observed, while the agreement for particle outlet concentration data is just qualitative;
- Size distribution of attached particles can be determined from the maximum retention function;
- Modelling-based predictions for high temperature geothermal conditions show that the maximum retention concentration decreases with temperature, yielding more severe permeability damage if compared with conventional aquifers and petroleum reservoirs.

Acknowledgements

Financial supports from the Australian Research Council (ARC) Discovery Project 1094299, ARC Linkage Projects 100100613 and 110200799, the Australian Renewable Energy Agency (ARENA), and the South Australian Centre for Geothermal Energy Research (SACGER) are gratefully acknowledged. Drs. Ulrike Schacht and Themis Carageorgos (University of Adelaide) are gratefully acknowledged for fruitful co-operation.

References

Aragón-Aguilar, A., Barragán-Reyes, R.M., Arellano-Gómez, V.M., 2013. Methodologies for analysis of productivity decline: a review and application. Geothermics 48, 69–79.

Badalyan, A., Carageorgos, T., You, Z., Schacht, U., Bedrikovetsky, P., Matthews, C., Hand, M.,2014. A new experimental procedure for formation damage assessment in geothermal wells. In: Proceedings, Thirty-Ninth Workshop on Geothermal Reservoir Engineering. Stanford University, California, USA.

Baudracco, J., 1990. Variations in permeability and fine particle migrations in unconsolidated sandstones submitted to saline circulations. Geothermics 19, 213–221.

Baudracco, J., Aoubouazza, M., 1995. Permeability variations in Berea and Vosges sandstone submitted to cyclic temperature percolation of saline fluids. Geothermics 24, 661–677.

Bedrikovetsky, P.G., 1993. Mathematical Theory of Oil & Gas Recovery. Kluwer Academic Publishers, London/Boston/Dordrecht.

Bedrikovetsky, P., 2008. Upscaling of stochastic micro model for suspension transport in porous media. Transp. Porous Media 75 (3), 335–369.
Bedrikovetsky, P., Siqueira, F.D., Furtado, C.A., Souza, A.L.S., 2011. Modified particle detachment model for colloidal transport in porous media. Transp. Porous Media 86, 353–383.
Bedrikovetsky, P., Zeinijahromi, A., Siqueira, F.D., Furtado, C.A., de Souza, A.L.S., 2012. Particle detachment under velocity alternation during suspension transport in porous media. Transp. Porous Media 91, 173–197.
Bradford, S.A., Torkzaban, S., Kim, H., Simunek, J., 2012. Modeling colloid and microorganism transport and release with transients in solution ionic strength. Water Resour. Res. 48, W09509.
Bradford, S.A., Torkzaban, S., Shapiro, A.A., 2013. A theoretical analysis of colloid attachment and straining in chemically heterogeneous porous media. Langmuir 29, 6944–6952.
Chauveteau, G., Nabzar, L., Coste, J.P., 1998. Physics and modeling of permeability damage induced by particle deposition. In: Proceedings – SPE International Symposium on Formation Damage Control, pp. 409–419.
Civan, F., 2007. Reservoir Formation Damage: Fundamentals, Modeling, Assessment, and Mitigation, 2nd ed. Gulf Publishing Company, Houston, Texas.
Cortis, A., Harter, T., Hou, L., Atwill, E.R., Packman, A.I., Green, P.G., 2006. Transport of *Cryptosporidium parvum* in porous media: long-term elution experiments and continuous time random walk filtration modeling. Water Resour. Res. 42, W12S13.
Derjaguin, B.V., Landau, L., 1941. Theory of the stability of strongly charged lyophobic sols and of the adhesion of strongly charged particles in solutions of electrolytes. Acta Phys. Chem. (URSS) 14, 633–662.
Freitas, A.M., Sharma, M.M., 2001. Detachment of particles from surfaces: an AFM study. J. Colloid Interface Sci. 233, 73–82.
García-García, S., Jonsson, M., Wold, S., 2006. Temperature effect on the stability of bentonite colloids in water. J. Colloid Interface Sci. 298, 694–705.
Ghassemi, A., Zhou, X., 2011. A three-dimensional thermo-poroelastic model for fracture response to injection/extraction in enhanced geothermal systems. Geothermics 40, 39–49.
Herzig, J.P., Leclerc, D.M., Legoff, P., 1970. Flow of suspensions through porous media – application to deep filtration. Ind. Eng. Chem. 62, 8–35.
Israelachvili, J.N., 2011. Intermolecular and Surface Forces, 3rd ed. Elsevier, Amsterdam, The Netherlands.
Jaya, M.S., Shapiro, S.A., Kristinsdottir, L.H., Bruhn, D., Milsch, H., Spangenberg, E., 2010. Temperature dependence of seismic properties in geothermal rocks at reservoir conditions. Geothermics 39, 115–123.
Jiao, D., Sharma, M.M., 1994. Mechanism of cake buildup in crossflow filtration of colloidal suspensions. J. Colloid Interface Sci. 162, 454–462.
Khilar, K.C., Fogler, H.S., 1998. Migrations of Fines in Porous Media. Kluwer Academic Publishers, Dordrecht, The Netherlands.
Kristinsdottir, L.H., Flovenz, O.G., Arnason, K., Bruhn, D., Milsch, H., Spangenberg, E., Kulenkampff, J., 2010. Electrical conductivity and P-wave velocity in rock samples from high-temperature Icelandic geothermal fields. Geothermics 39, 94–105.
Lever, A., Dawe, R.A., 1984. Water-sensitivity and migration of fines in the Hopeman Sandstone (Scotland). J. Pet. Geol. 7, 97–107.
Logan, J.D., 2001. Transport Modeling in Hydrogeochemical Systems. Springer, New York.
Marquardt, D., 1963. An algorithm for least-squares estimation of nonlinear parameters. J. Soc. Ind. Appl. Math. 11, 431–441.
Mays, D., Hunt, J., 2005. Hydrodynamic aspects of particle clogging in porous media. Environ. Sci. Technol. 39, 577–584.
Mays, D., Hunt, J., 2007. Hydrodynamic and chemical factors in clogging by montmorillonite in porous media. Environ. Sci. Technol. 41, 5666–5671.
Milsch, H., Kristinsdottir, L.H., Spangenberg, E., Bruhn, D., Flovenz, O.G., 2010. Effect of the water-steam phase transition on the electrical conductivity of porous rocks. Geothermics 39, 106–114.
Miranda, R.M., Underdown, D.R.,1993. Laboratory measurement of critical rate: a novel approach for quantifying fines migration problems. In: SPE Production Operations Symposium, 21–23 March. Society of Petroleum Engineers, Oklahoma, OK.
Nabzar, L., Chauveteau, G., 1997. Permeability damage by deposition of colloidal particles. In: SPE – European Formation Damage Control Conference, Proceedings, pp. 161–168.
Ochi, J., Vernoux, J.F., 1998. Permeability decrease in sandstone reservoirs by fluid injection: hydrodynamic and chemical effects. J. Hydrol. 208, 237–248.
Oliveira, M., Vaz, A., Siqueira, F., Yang, Y., You, Z., Bedrikovetsky, P., 2014. Slow migration of mobilised fines during flow in reservoir rocks: laboratory study. J. Pet. Sci. Eng. 122, 534–541.
Pang, S., Sharma, M.M., 1997. A model for predicting injectivity decline in water-injection wells. SPE Form. Eval. 12, 194–201.
Priisholm, S., Nielsen, B.L., Haslund, O., 1987. Fines migration, blocking, and clay swelling of potential geothermal sandstone reservoirs, Denmark. SPE Form. Eval. 2, 168–178.
Rahman, S.S., Arshad, A., Chen, H., 1994. Prediction of critical condition for fines migration in petroleum reservoirs. In: SPE Asia Pacific Oil and Gas Conference, Society of Petroleum Engineers, Melbourne, Australia, 7–10 November.
Rosenbrand, E., Fabricius, I.L., 2012. Effect of hot water injection on sandstone permeability: an analysis of experimental literature. In: SPE Europec/EAGE Annual Conference, Copenhagen, Denmark.
Rosenbrand, E., Fabricius, I.L., Kets, F.,2013. Kaolinite mobilisation in sandstone: pore plugging vs suspended particles. In: Proceedings, Thirty-Eighth Workshop on Geothermal Reservoir Engineering. Stanford University, CA, USA.
Rosenbrand, E., Fabricius, I.L., Yuan, H.,2012. Thermally induced permeability reduction due to particle migration in sandstones: the effect of temperature on kaolinite mobilisation and aggregation. In: Proceedings, Thirty-Seventh Workshop on Geothermal Reservoir Engineering. Stanford University, California, USA.
Rosenbrand, E., Haugwitz, C., Jacobsen, P.S.M., Kjøller, C., Fabricius, I.L., 2014. The effect of hot water injection on sandstone permeability. Geothermics 50, 155–166.
Rosenbrand, E., Kjøller, C., Riis, J.F., Kets, F., Fabricius, I.L., 2015. Different effects of temperature and salinity on permeability reduction by fines migration in Berea sandstone. Geothermics 53, 225–235.
Rousseau, D., Hadi, L., Nabzar, L., 2008. Injectivity decline from produced-water reinjection: new insights on in-depth particle-deposition mechanisms. SPE Prod. Oper. 23, 525–531.
Schechter, R.S., 1992. Oil Well Stimulation. Prentice Hall, Englewood Cliffs, NJ.
Schembre, J.M., Kovscek, A.R., 2005. Mechanism of formation damage at elevated temperature. J. Energy Resour. Technol. Trans. ASME 127, 171–180.
Schijven, J.F., Hassanizadeh, S.M., 2000. Removal of viruses by soil passage: overview of modeling, processes, and parameters. Crit. Rev. Environ. Sci. Technol. 30, 49–127.
Sefrioui, N., Ahmadi, A., Omari, A., Bertin, H., 2013. Numerical simulation of retention and release of colloids in porous media at the pore scale. Colloids Surf. A: Physicochem. Eng. Asp. 427, 33–40.
Shapiro, A.A., 2007. Elliptic equation for random walks. Application to transport in microporous media. Phys. A: Stat. Mech. Appl. 375, 81–96.
Shapiro, A.A., Wesselingh, J.A., 2008. Gas transport in tight porous media. Gas kinetic approach. Chem. Eng. J. 142, 14–22.
Shapiro, A.A., Yuan, H., 2013. Application of stochastic approaches to modeling suspension flow in porous media. In: Skogseid, A., Fasano, V. (Eds.), Statistical Mechanics and Random Walks: Principles, Processes and Applications. Nova Science Publishers, Inc., New York, USA, pp. 1–38.
Sharma, M.M., Pang, S., Wennberg, K.E., Morgenthaler, L.N., 2000. Injectivity decline in water-injection wells: an offshore gulf of Mexico case study. SPE Prod. Facil. 15, 6–13.
Sharma, M.M., Yortsos, Y.C., 1987a. Transport of particulate suspensions in porous media: model formulation. AIChE J. 33, 1636–1643.
Sharma, M.M., Yortsos, Y.C., 1987b. Fines migration in porous media. AIChE J. 33, 1654–1662.
Tikhonov, A.N., Samarskii, A.A., 2013. Equations of Mathematical Physics. Dover Publications.
Tufenkji, N., 2007. Colloid and microbe migration in granular environments: a discussion of modelling methods. In: Frimmel, F.H., von der Kammer, F., Flemming, H.-C. (Eds.), Colloidal Transport in Porous Media. Springer, Berlin, Germany, pp. 119–142.
Tufenkji, N., Elimelech, M., 2004. Correlation equation for predicting single-collector efficiency in physicochemical filtration in saturated porous media. Environ. Sci. Technol. 38, 529–536.
Verwey, E.J.W., Overbeek, J.T.G., 1948. Theory of the Stability of Lyophobic Colloids. Elsevier, Amsterdam.
You, Z., Badalyan, A., Bedrikovetsky, P., 2013. Size-exclusion colloidal transport in porous media – stochastic modeling and experimental study. SPE J. 18, 620–633.
You, Z., Badalyan, A., Yang, Y., Bedrikovetsky, P., Hand, M., 2014. Laboratory study of fines migration in geothermal reservoirs. Geothermics (submitted for publication).
Yuan, H., Shapiro, A.A., 2011. A mathematical model for non-monotonic deposition profiles in deep bed filtration systems. Chem. Eng. J. 166, 105–115.
Yuan, H., Shapiro, A.A., 2012. Colloid transport and retention: recent advances in colloids filtration theory. In: Ray, P.C. (Ed.), Colloids: Classification, Properties and Applications. Nova Science Publishers, Inc., New York, USA, pp. 201–242.
Yuan, H., You, Z., Shapiro, A., Bedrikovetsky, P., 2013. Improved population balance model for straining-dominant deep bed filtration using network calculations. Chem. Eng. J. 226, 227–237.

Please cite this article in press as: You, Z., et al., Mathematical modelling of fines migration in geothermal reservoirs. Geothermics (2015), http://dx.doi.org/10.1016/j.geothermics.2015.05.008